Journal of Molecular Catalysis A: Chemical 317 (2010) 34–40

Contents lists available at ScienceDirect

Journal of Molecular Catalysis A: Chemical

journal homepage: www.elsevier.com/locate/molcata

Synthetic $Bi_2O_2CO_3$ nanostructures: Novel photocatalyst with controlled special surface exposed

Yan Zheng, Fang Duan, Mingqing Chen, Yi Xie*

School of Chemical and Material Engineering, Jiangnan University, Lihu Road, 1800#, Wuxi, Jiangsu 214122, PR China

ARTICLE INFO

Article history:
Received 22 September 2009
Received in revised form 14 October 2009
Accepted 14 October 2009
Available online 23 October 2009

Keywords:
$Bi_2O_2CO_3$
Special exposed surface
Photocatalytic activity

ABSTRACT

In this work a novel $Bi_2O_2CO_3$ photocatalyst was first put forward by virtue of structural understanding. In particular, the flower-like $Bi_2O_2CO_3$ hierarchitecture with the controlled special {0 0 1} plane exposed was first synthesized via a mild route, showing the excellent photocatalytic activity due to the large distortion of Bi–O on the exposed surface. The $Bi_2O_2CO_3$ nanostructures have proved to be not only a new photocatalyst under solar light irradiation, but also a possible example for investigating the key factors of which may impact on the photocatalytic ability. The results confirmed that the higher efficiency of the photocatalytic activity should be contributed synergistically by the higher BET surface area and the special exposed surface.

© 2009 Published by Elsevier B.V.

1. Introduction

Since 1972 Fujishima and Honda reported TiO_2 as photocatalyst splitted water into oxygen and hydrogen [1], much admirable researches on the preparation of the environmentally friendly photocatalysts have been investigated to progress the activity of the photocatalysts [2–4] by the energy shortage and environment pollution of the whole globe recently [5–8]. Meanwhile, the factors which may impact the catalysis properties have attracted more and more intensive attention accompanied. Many works have put forward that the high BET surface areas are the main influencing factor for the catalysis [4]. For example, Zhao reported that the porous tin dioxide nanostructures with high surface areas exhibit excellent catalytic activity toward methanol decomposition [9]. Nevertheless, recent researches have indicated that the particular plane may also be pivotal to the catalytic activity [10–14]. For instance, in the case of the iron catalysts used for the synthesis of ammonia, the preferentially exposed {1 1 1} planes of the iron surface were observed to be crucial to generate excellent activity [15]. The monoclinic scheelite $BiVO_4$ was reported to show much higher photocatalytic activity under visible light irradiation which was mainly attributed to basal plane of (0 1 0) with the distorted the Bi–O polyhedron [16]. Very recently our group have pointed out that the γ-Bi_2MoO_6 with the preferentially exposed {0 1 0} plane show excellent photocatalytic activity under the visible light, due to that the particular reactive plane with much more oxygen defects and in-plane vacancies, derived from the large distortion of the MoO_6 octahedra, play a more important role of the enhanced photocatalytic activity [17].

In recent years, the bismuth-containing materials with layered structure have attracted much attention for their admirable photocatalytic properties under the solar light, among which aurivillius structures which have an intergrowth of $[Bi_2O_2]^{2+}$ layers and $[A_mB_{m-1}O_{3m+1}]^{2-}$ perovskite-type sheets are one of the most appealing candidates [18,19]. In this sense, the "Sillén" phase compounds with less attention could be worth expecting as potential photocatalysts especially because of the similarities in structure with the aurivillius phase (the presence of $[Bi_2O_2]^{2+}$ layers) [20]. The "sillén" phase which was named by its discoverer was initially considered as a series of bismuth oxyhalides, but later extended to a larger family such as Pb, W and Sb oxyhalides, carbonate, and ketterite. The sillén structure with the general formula $[Bi_2O_2]$ $[X_m]$ (X = halogen or other ion group) usually possess alternating $[Bi_2O_2]^{2+}$ sheets and the X slabs (m = 1, 2 or 3 rarely) [21,22]. Currently, the sillén structure BiOX (X = Cl, Br, I) nanoplates were synthesized via a general one-pot solvothermal process and very promising photocatalysts for degrading organic pollutants by Zhang et al. [23].

The bismutite ($Bi_2O_2CO_3$) first reported by Grice's group [19] is a typical "sillén" phase, in which Bi–O layers and (CO_3) layers are intergrown with the plane of the (CO_3) group orthogonal to the plane of the Bi–O layer. The segregated "standing-on-end" carbonate layer can be clearly seen in the crystal structure of the $Bi_2O_2CO_3$ as shown in Fig. 1. Also, one can easily find that the large cation Bi^{3+} with [8]-coordination shows stereo active lone-pair behaviors that may result in the Bi–O polyhedron with large distortion [24].

* Corresponding author.
E-mail address: yxie@jiangnan.edu.cn (Y. Xie).

1381-1169/$ – see front matter © 2009 Published by Elsevier B.V.
doi:10.1016/j.molcata.2009.10.018

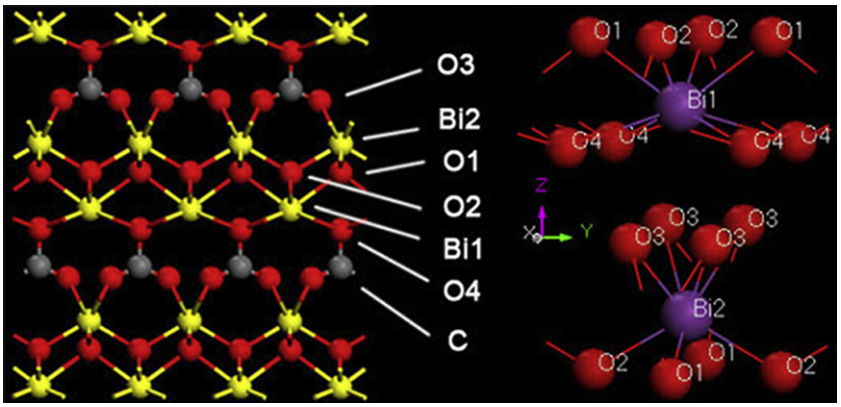

Fig. 1. The structure of the bismutite ($Bi_2O_2CO_3$) with the (1 0 0) crystal plane and the large cation (Bi) coordinations in oblique projection with [0 0 1] vertical.

By the structural analyses, obviously there is a great potential for the $Bi_2O_2CO_3$ with layered structure used as photocatalyst. Meanwhile, previous applications of $Bi_2O_2CO_3$ were only be restricted in medicine and microelectrode, as far as we know [25,26]. Furthermore, the internal layered structure of a material would guide the lower growth rate along certain axis compared with that for other axes, to form 2D morphologies such as sheet-like/plate-like morphologies. The highly anisotropic internal structure of $Bi_2O_2CO_3$ is obviously a benefit for controlling the formation of $Bi_2O_2CO_3$ sheet-like or plate-like nanounits with special plane. On the other hand, previous work was indicated that controlled organization of primary building units into hierarchically structured nanoarchitecture represents another challenge for their high potential in applications [27,28]. So the $Bi_2O_2CO_3$ with hierarchical structure assembled by nanosheets or nanoplates are expected to show more effective photocatalysis.

Herein, we report a facile method to fabricate a series of $Bi_2O_2CO_3$ samples with different morphologies and then investigate their photocatalytic properties for degrading the organic pollutants under the solar light. The $Bi_2O_2CO_3$ flower-like hierarchitecture with exposed {0 0 1} plane perform admirable photocatalytic activity. Based on the close correlation between the physicochemical properties and the structure characteristics of the material, the $Bi_2O_2CO_3$ has proved to be not only a new photocatalyst under solar light irradiation, but also a possible example for investigating the key factors of which may impact on the photocatalytic ability.

2. Experimental

2.1. Synthesis method

For the flower-like $Bi_2O_2CO_3$ hierarchitecture sample, $Bi(NO_3)_3{\cdot}5H_2O$ and $C_6H_8O_7{\cdot}H_2O$ of analytic grade purity were purchased from Shanghai Chemical Co. Ltd. and were used as received. To obtain flower-like sample, 1.5 mmol $Bi(NO_3)_3{\cdot}5H_2O$ was dissolved into dilute HNO_3 solution, and then 1 mmol citric acid was added into the above solution which was stirred for about 10 min until a clear solution formed. Finally, the pH value of the solution was adjusted to 7–9 using 2.0 mol L^{-1} NaOH solution under stirring. The final transparent solution was transferred into a Teflon-sealed autoclave and maintained at 180 °C for 24 h. The gray product with flower-like hierarchitecture was isolated by centrifugation, washed with distilled water and absolute ethanol for several times, and finally dried in a vacuum at 50 °C for 5 h.

The sponge-like $Bi_2O_2CO_3$ porous spheres were obtained while the pH value of the precursor solution was adjusted to 4–5 with the other conditions unchanged. The plate-like sample was obtained while the reaction temperature increased to 200 °C with the other conditions unchanged.

2.2. Characterization

The phase and purity of these obtained samples was characterized by the X-ray diffraction (XRD) pattern, which was recorded on a Rigaku Dmax diffraction system using a Cu Kα source with $\lambda = 1.54187$ Å. The scanning electron microscopy (SEM) images were taken using a Sirion 200 field emission scanning electron microscope (FE-SEM, 20 kV). Transmission electron microscopy (TEM) images and high-resolution transmission electron microscopy (HR-TEM) images were obtained with a Hitachi 800 system at 200 kV and a JEOL-2010 system also at 200 kV.

2.3. Photocatalytic experiment

Photocatalytic activity of the obtained $Bi_2O_2CO_3$ samples was investigated by photocatalytic degradation of N,N,N′,N′-tetraethylated Rhodamine (RhB) under the visible light irradiation which was provided by a 1000 W Xe lamp. 0.08 g of $Bi_2O_2CO_3$ was added into 100 mL RhB solution (10^{-5} mol L^{-1}). The solution was stirred magnetically in the dark for 8 h, and then exposed to the lamp under magnetic stirring. After irradiation for a given time, the suspensions were centrifuged to separate the $Bi_2O_2CO_3$, and the RhB concentration of the filtrate was determined using the Lambda-35 UV–vis spectrometer.

3. Results and discussion

3.1. Structural characterization of the prepared $Bi_2O_2CO_3$ samples

The phase and purity of the samples were determined by X-ray powder diffraction (XRD), and the typical diffraction patterns are shown in Fig. 2. All of the peaks in XRD patterns of the three samples could be readily indexed to the bismuth oxide carbonate, with lattice constants of $a = b = 3.865$ Å and $c = 13.67$ Å, which is found to match well with the standard XRD patterns for $Bi_2O_2CO_3$ (JCPDS card No. 411488). The significantly intensified (1 1 0) diffraction peaks of flower-like sample compared with the other characteristic diffraction peaks of $Bi_2O_2CO_3$ reveal that there is a bias of orientations of {1 1 0} crystallographic plane. Meanwhile, it was clearly shown that the XRD peaks of sponge-like porous spheres were a broader band characteristic which is due to the distortion of lattice caused by the microstrain effects. The sharp and strong peaks of the plate-like sample indicated good crystallinity of the product as well as large particles.

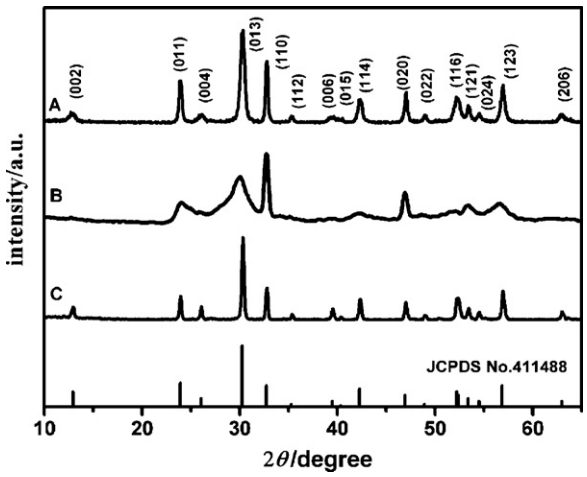

Fig. 2. XRD pattern of the as-prepared $Bi_2O_2CO_3$ samples: (A) flower-like sample obtained at pH = 7–8 and 180 °C; (B) sponge-like porous sphere sample obtained at pH = 4–5 and 180 °C; (C) plate-like sample obtained at pH = 7–8 and 200 °C.

The morphologies of bismuth oxide carbonate samples are illuminated by FE-SEM, TEM and HR-TEM as shown in Figs. 3 and 4, in which it can be clearly seen that the flower-like sample with the size of 2 μm are consisted of small flakes. The HR-TEM image of an individual flake of the flower-like $Bi_2O_2CO_3$ hierarchitecture sample as shown in Fig. 4A indicates their single-crystalline nature and the calculated lattice spacing of 2.75 Å and 2.74 Å correspond to the literature data of $d_{1\,1\,0}$ = 2.734 Å and $d_{\bar{1}\,1\,0}$ = 2.734 Å, respectively. This phenomenon is also consistent with the XRD observation that the significantly intensified (1 1 0) diffraction peaks compared with the characteristic (0 1 3) diffraction peak of $Bi_2O_2CO_3$. These results also revealed that the exposed basal plane is a (0 0 1) plane, featuring a square arrangement of atoms along with the instinct layer. Moreover, the selected-area electron-diffraction (SAED) patterns (Fig. 4A inset) indicate that the clear diffraction spots with well alignment further point out the single-crystal nature of the flakes and the bias of orientation of [0 0 1] also explains the intensified (1 1 0) peaks in the XRD pattern. All the above characterizations give that the flakes of flower-like $Bi_2O_2CO_3$ sample with a preferred [0 0 1] orientation and the wide surface of the flakes can be indexed as {0 0 1} plane.

As shown in Fig. 3C and D the obtained sponge-like porous spheres with the size of 6–8 μm possess meso/macro-porous structure. From the SEM image and TEM image there seemed to be many pores with different sizes either on the surface or inside the sponge-like porous spheres, both of which endow the sample with a large surface-to-volume ratio. The sponge-like porous spheres are indeed polycrystalline reflected by the contrast HR-TEM image and SAED rings as shown in Fig. 4B. The HR-TEM image of the sponge-like porous sphere indicates that the porous spheres are

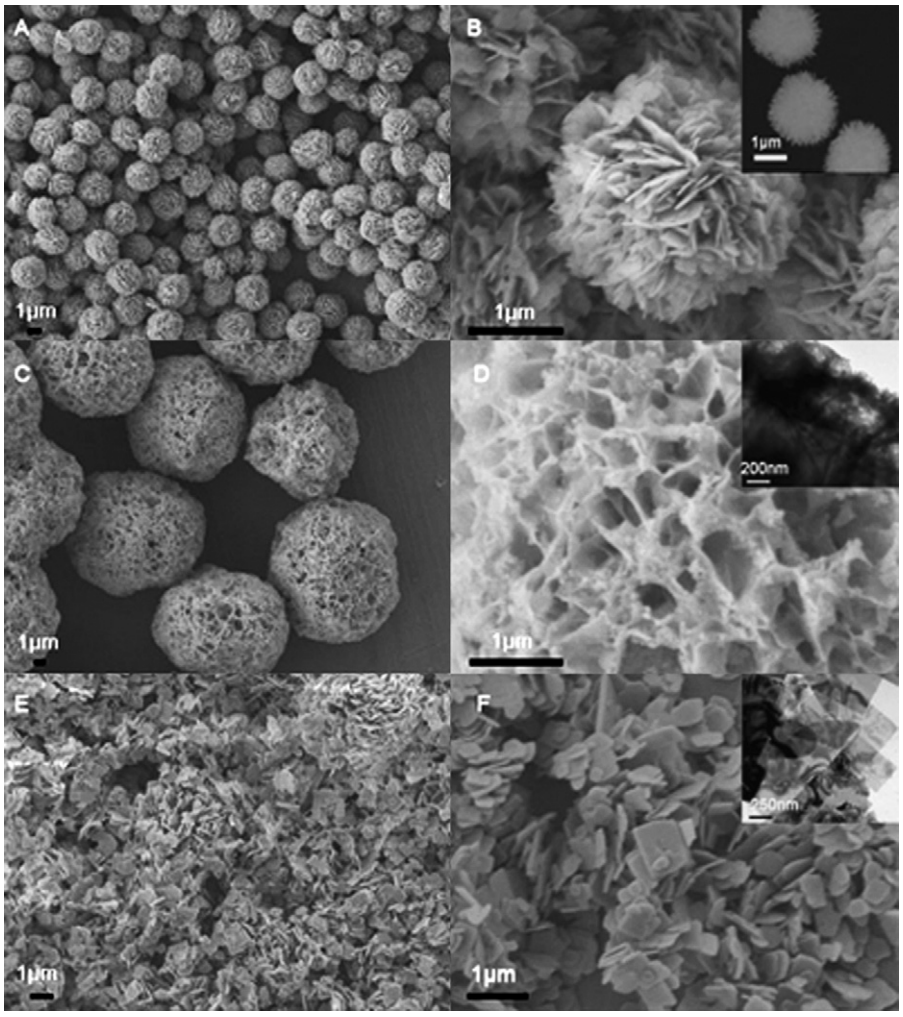

Fig. 3. The SEM images of the $Bi_2O_2CO_3$ samples: (A and B), flower-like sample; (C and D), sponge-like porous spheres sample; (E and F), plate-like sample, and inset in (B, D and F) are the corresponding TEM images.

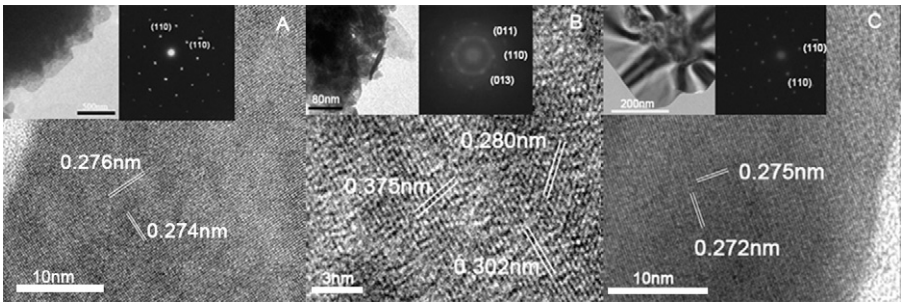

Fig. 4. The HR-TEM image of the $Bi_2O_2CO_3$ samples: (A) flower-like sample; (B) sponge-like porous sphere sample and (C) plate-like sample (left inset: TEM image. right inset: SAED pattern).

composed of fine crystallites in a size range of only 3–5 nm. These particles were well crystallized, as shown by clear lattice fringes ($d_{0\,1\,1}$ = 0.37 nm, $d_{0\,1\,3}$ = 0.30 nm, $d_{1\,1\,0}$ = 0.28 nm, etc.) and relatively sharp selected-area electron-diffraction (SAED) rings in the Fig. 4C inset.

From Fig. 3E and F, it is clearly seen that the size of the plate-like sample with the size of 500–800 nm is much larger than the flakes of the flower-like sample which may make lower BET surface area of the plate-like sample than the other samples. In Fig. 4C, The HR-TEM image of the plate-like sample indicates that the exposed surface of the sheets also can be indexed as {0 0 1} plane and the SAED pattern (Fig. 4C inset) also reveals the clear diffraction spots with well alignment show the single-crystal character of the plate-like sample.

3.2. The formation mechanism of $Bi_2O_2CO_3$ nanostructures

In this approach, $Bi_2O_2CO_3$ nanostructures formed via the hydrothermal reaction of the $Bi(NO_3)_3{\cdot}5H_2O$ and $C_6H_8O_7{\cdot}H_2O$ solution, in which the bismuth citrate sol were firstly obtained with continuous stirring at the room temperature. The formation of bismuth citrate sol can be supported by the observation that when stirred, the solution of the $Bi(NO_3)_3{\cdot}5H_2O$ and $C_6H_8O_7{\cdot}H_2O$ became opalescent and finally clear, and then the Tyndall effect was observed using a light beam from a commercial laser pointer, as shown in Fig. 5. Since the decomposition of bismuth citrate need high temperature as high as 280 °C [29], in our approach, the $Bi_2O_2CO_3$ should be formed from the combination of $(BiO)^+$ ion from the dehydration of $Bi(NO_3)_2$ and carbonate ion from the dissolved CO_2 which was decomposed from citric ion. The formation of the bismuth citrate sol played an important role in the controlled releasing of $(BiO)^+$ and $(CO_3)^{2-}$, which is profit for the conformation of the $Bi_2O_2CO_3$ nanounits. With the temperature increased to 180 °C, the citric acid was gradually decomposed to generate the CO_2 and then the CO_2 was dissolved in the water and hydrolyzed to the carbonate ion, which was then combined with the $(BiO)^+$ generated from the hydrolysis of the Bi^{3+}. The whole involved reactions can be described as follows.

$$Bi^{3+} + C_6H_5O_7{}^{3-} \rightleftharpoons C_6H_5O_7Bi \quad (1)$$

$$C_6H_8O_7 \Rightarrow CO_2 + H_2O \rightleftharpoons CO_3{}^{2-} + 2H^+ \quad (2)$$

$$Bi^{3+} + H_2O \rightleftharpoons BiO^+ + 2H^+ \quad (3)$$

$$2BiO^+ + CO_3{}^{2-} \Rightarrow Bi_2O_2CO_3\downarrow \quad (4)$$

Several experiments through intercepting the intermediate products were performed in the different stages and the intermediate products were inspected by FE-SEM as shown in Scheme 1. In the formation of flower-like $Bi_2O_2CO_3$ nanostructures, only amorphous floccules can be observed in the initial stage as indicated in Scheme 1A. When the reaction time was prolonged, it is observed that the amorphous floccules assembled into a flaky agglomeration, and interestingly, the embryo of the hierarchical flowers of $Bi_2O_2CO_3$ have been formed in flaky agglomeration. As the reaction time increases, more flakes grow, and the flakes agglomerations disappeared gradually that well-defined hierarchical $Bi_2O_2CO_3$ flowers with good crystallinity are aged for 24 h. On the other hand, when the pH value of the precursor solution is adjusted to 3–4, just as shown in Scheme 1B, only some very small particles (~30 nm) formed at the primary stage and with the reaction time prolonged the proportion of the small sheets greatly increased coexisting with the nanoparticles. After Oswald ripening process for enough time, the sponge sphere with a 3D porous morphology was being formed. While the reaction temperature was increased to 200 °C, only plate-like product was obtained, as indicated at Scheme 1C.

To investigate the effect of reaction conditions on the formation of $Bi_2O_2CO_3$ flower-like hierarchitecture, a series of comparative experiments were carried out through the typical process. When the reaction was processed without the citric acid, the $Bi_2O_2CO_3$ were not obtained. Yet, when the reaction with tri-sodium citrate instead of citrate with the other conditions unchanged, the flower-like $Bi_2O_2CO_3$ sample were also obtained, indicating that the citric group is the key factor to supply $CO_3{}^{2-}$ in the formation of the flower-like $Bi_2O_2CO_3$ hierarchitecture. When the reaction temperature is decreased to 150 °C, the $Bi_2O_2CO_3$ sample with flower-like

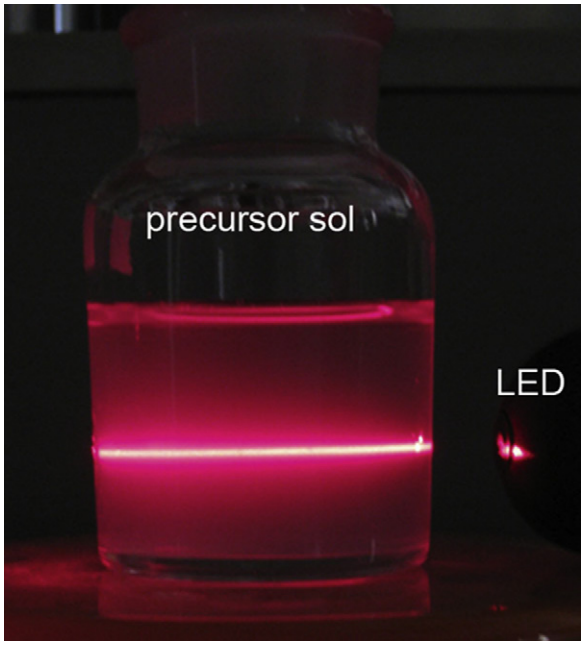

Fig. 5. The Tyndall effect of the precursor ($C_6H_5O_7Bi$) sol was observed using a Light Emitting Diode (LED).

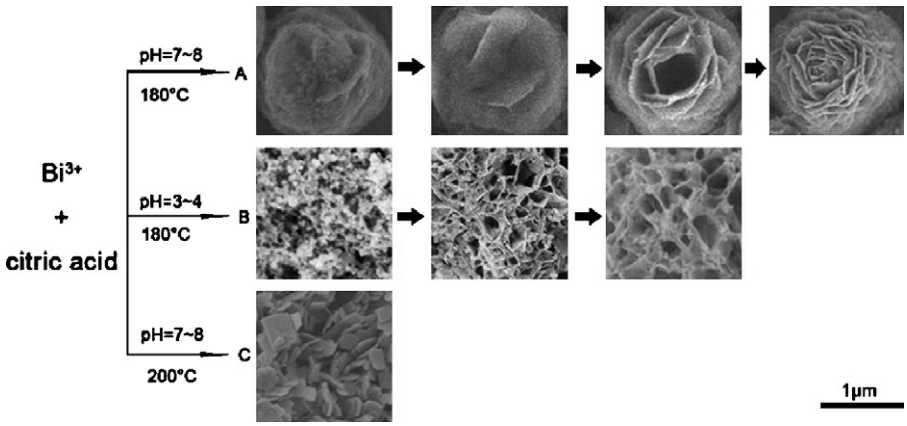

Scheme 1. The SEM images of the different stages of $Bi_2O_2CO_3$ samples with different morphologies: (A) flower-like sample; (B) sponge-like porous sphere sample; (C) plate-like sample.

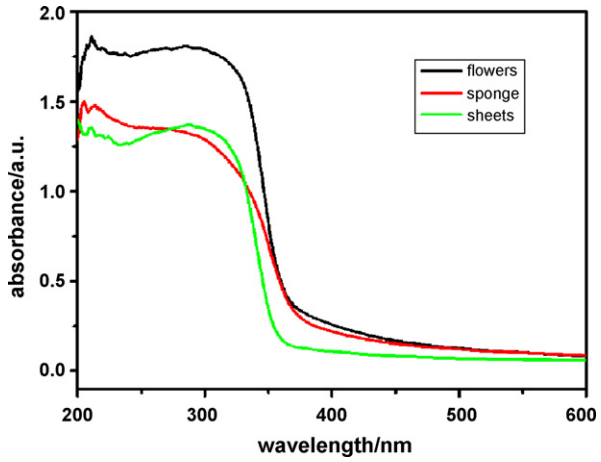

Fig. 6. UV–visible diffuse reflectance spectra of the prepared $Bi_2O_2CO_3$ samples.

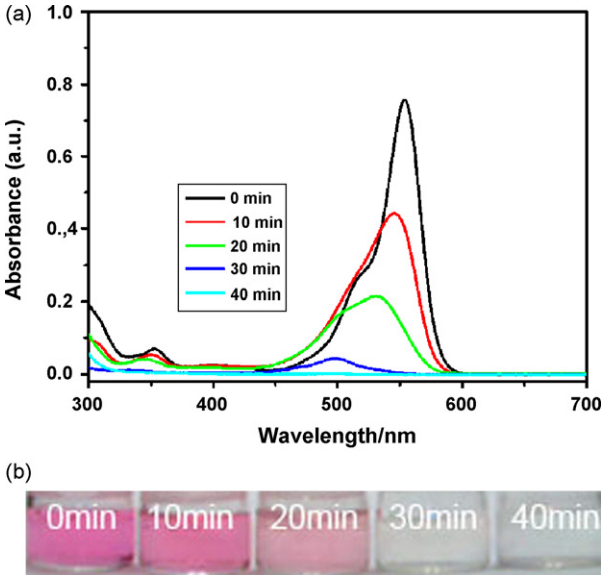

Fig. 7. The temporal evolution of the spectra during the photodegradation of RhB (initial concentration: 10^{-5} mol/L, 100 mL) and the photos of the RhB solution color changed through the increasing time in the presence of the flower-like $Bi_2O_2CO_3$ hierarchitecture sample.

architecture cannot be obtained, further proving the temperature also is the crucial point to the $Bi_2O_2CO_3$ flower-like architecture, because the citric gel might be completely decomposed over 170 °C. With the temperature increased to 180 °C the citric gel was gradually decomposed and the carbon dioxide was released slowly to offer the carbonate ion to build the $Bi_2O_2CO_3$ architecture. While the temperature of the reaction increased to 200 °C, the citric gel was decomposed too quickly to build the $Bi_2O_2CO_3$ hierarchitecture.

3.3. UV–vis DRS and BET analysis of the prepared $Bi_2O_2CO_3$ samples

To estimate the band gaps of the photocatalysts, the UV–visible diffuse reflectance spectra (DRS) of the above prepared $Bi_2O_2CO_3$ samples were measured by using a UV–vis spectrometer, as shown in Fig. 6, in which the photoabsorption of the all three samples was in the range of from the UV light region to visible light shorter than 480 nm. The steep shape of the spectra indicates that the visible light absorption is not due to the transition from the impurity level but is due to the band-gap transition [30]. Following the equation $ah\nu = A(h\nu - Eg)^{n/2}$ [20], the band gaps of the above samples which were estimated from the onset of the absorption edge are about 3.1 eV. The band gap makes the $Bi_2O_2CO_3$ a potential photocatalyst for degradating the organic pollutants under solar light irradiation.

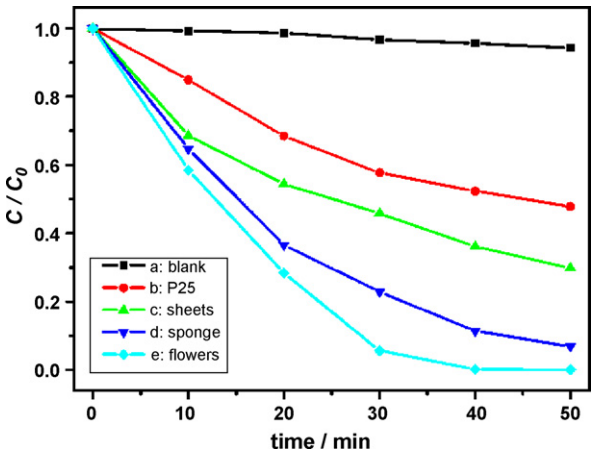

Fig. 8. The photocatalytic degradation of the fully N,N,N′,N′-tetraethylated rhodamine under the visible light irradiation in the presence of the prepared $Bi_2O_2CO_3$ samples.

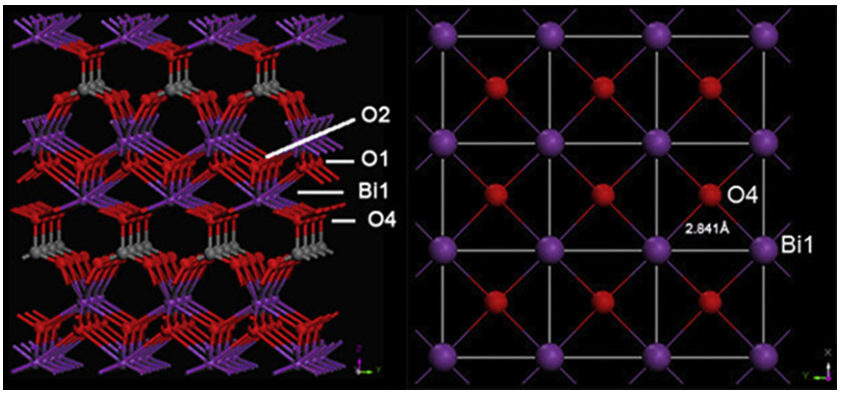

Fig. 9. The (0 0 1) surface of $Bi_2O_2CO_3$ shows the terminology used for difference types of surface atoms.

The BET surface areas of the as-obtained $Bi_2O_2CO_3$ samples are expected to be different for various morphologies and sizes. The BET surface area of the flower-like sample was 20.43 m^2/g, whereas that of the sponge-like porous sphere sample was 50.60 m^2/g and the plate-like sample was 4.30 m^2/g. Clearly, the sponge-like porous spheres possess the largest BET surface area due to the lots of pores existed at different size on the surface or inside the sponge-like porous spheres, which may be potentially assistant for the photocatalysis. It is reasonable that the BET surface area of the plated-like sample was only 20% of the flower-like sample due to its larger size.

3.4. Photocatalytic activity of the prepared $Bi_2O_2CO_3$ samples

The photocatalysis tests indicate that all $Bi_2O_2CO_3$ samples are good photocatalysts on degradation of the RhB solution under the artificial solar light irradiation, as we expected. The photodegradation process of RhB was recorded by the temporal evolution of the spectra and all of the samples displayed the similar procedure. As an example shown in Fig. 7 with the presence of flower-like $Bi_2O_2CO_3$ hierarchitecture, during the process of RhB dye decomposition in water solution under solar light irradiation, the intense pink color of the starting RhB solution almost faded completely only with the exposure time increasing to 50 min. The absorption peaks at 554 nm corresponding to RhB diminished gradually with an absorption band shift to shorter wavelengths obviously as the exposure time was extended. At last, no new absorption bands show in either the visible or ultraviolet regions, which point out the complete photodegradation of RhB. Apparently, solar light irradiation of the RhB/$Bi_2O_2CO_3$ dispersions with different morphological samples led to different photodegradation rates of RhB, as shown in Fig. 8 indicating the different photocatalytic performances of these $Bi_2O_2CO_3$ samples. It is obviously seen that under identical conditions the flower-like sample exhibit much greater activity than that of other $Bi_2O_2CO_3$ samples. The blank test demonstrates that the degradation of RhB is extremely slow without any photocatalyst under the solar light irradiation (Fig. 8a), meanwhile P25 is less active under the solar light irradiation (Fig. 8b). Clearly, the photodegradation efficiency of RhB is not simply enhanced with the increasing BET surface area of the $Bi_2O_2CO_3$ photocatalysts.

Notably, the sponge-like porous sphere sample with the double BET surface area than the flower-like sample did not exhibit the best efficiency, which strongly demonstrated that larger BET surface area does not mean the better photocatalytic properties, while the flower-like $Bi_2O_2CO_3$ sample exhibit the excellent photocatalytic properties with less than half of the BET surface area of $Bi_2O_2CO_3$ sponge-like porous sphere sample. This interesting phenomenon drives us for closer attention: are there any other vital factors for the higher photocatalytic efficiency? For further understanding the factors of impacting on the photocatalytic properties, the structure of the stoichiometric bismuth oxide carbonate (0 0 1) plane was investigated in Fig. 9, where we indicated the terminology used for different kinds of surface atoms and the striking feature of the surface. On the preferentially exposed {0 0 1} plane of $Bi_2O_2CO_3$ flakes, the Bi–O square anti-prism with [8]-coordination compressed along the *c*-axis supply lots of defects formed from the unstable oxygen which have the unstable bond with the Bi atoms in the $Bi_2O_2CO_3$ crystal structure. With the irradiation of the solar light, on the preferentially exposed {0 0 1} plane of the $Bi_2O_2CO_3$, especially the Bi1–O4 with the longest bond may mainly supply oxygen defects. In addition, the thinness of the flake-like nanounit also contribute on the distortion of Bi–O polyhedron, in that electron–holes generated inside the crystal easily transfer to the surface for the relatively large distortion of the Bi–O polyhedron and react with the RhB. In this case, the flower-like $Bi_2O_2CO_3$ hierarchitecture assembled by nanosheets or nanoplates with more effective {0 0 1} plane exposing the distorted Bi–O polyhedron exhibit the excellent photodegradation efficiency. Meanwhile, the plate-like sample shows lower activity because of the much lower BET surface area. In addition, though the sponge sphere sample possesses more than double BET surface area of the flower-like sample, it do not show higher efficiency because of its lower effective surface exposed. In a word, the high efficiency of the photocatalytic activity should be contributed synergistically by the high BET surface area and the special exposed surface, namely the higher BET surface area of the special effective surface exposed is most preferable to improve the photocatalysis.

4. Conclusions

In summary, the $Bi_2O_2CO_3$ samples as a new photocatalyst with different morphologies and surface structure features were prepared via a simple hydrothermal route and their photocatalytic properties were investigated by degrading the RhB under solar light irradiation. The exposed reactive {0 0 1} plane of the flower-like hierarchitecture $Bi_2O_2CO_3$ assembled by nanoflakes may contribute much more to the enhanced photocatalytic activity except the higher BET surface area because the Bi–O square anti-prism with [8]-coordination compressed along the *c*-axis supply lots of oxygen defects which is more preferred to generate the electron and vacancy. Thus, the as-obtained $Bi_2O_2CO_3$ nanostructures have been proved to be not only a new kind of photocatalysts under solar light irradiation, but also provide an excellent example for investigating the key factors of which may impact on the photocatalysis for future applications.

Acknowledgment

This work was supported by the National Natural Science Foundation of China (20671043).

References

[1] A. Fujishima, K. Honda, Nature 238 (1972) 37–38.
[2] A.T. Bell, Science 299 (2007) 1688–1691.
[3] H.X. Li, Z.F. Bian, J. Zhu, Y.F. Lu, J. Am. Chem. Soc. 129 (2007) 4538–4539.
[4] Y. Zhou, M. Antonietti, J. Am. Chem. Soc. 125 (2003) 14960–14961.
[5] L.S. Zhang, W.Z. Wang, Z.G. Chen, L. Zhou, J. Mater. Chem. 17 (2007) 2526–2532.
[6] C. Zhang, Y.F. Zhu, Chem. Mater. 17 (2005) 3537–3545.
[7] Y. Zheng, J. Wu, F. Duan, Y. Xie, Chem. Lett. 36 (2007) 520–521.
[8] H.B. Fu, C.S. Pan, W.Q. Yao, Y.F. Zhu, J. Phys. Chem. B 109 (2005) 22432–22439.
[9] Q.R. Zhao, Z.G. Zhang, Y. Xie, J. Phys. Chem. B 110 (2006) 15152–15156.
[10] K. Zhou, X. Wang, X.M. Sun, Q. Peng, Y.D. Li, J. Catal. 229 (2005) 206–212.
[11] L.H. Hu, Q. Peng, Y.D. Li, J. Am. Chem. Soc. 130 (2008) 16136–16137.
[12] D.O. Scanlon, N.M. Galea, B.J. Morgan, G.W. Watson, J. Phys. Chem. C 113 (2009) 11095–11103.
[13] E. Aneggi, J. Llorc, M. Boaro, A. Trovarelli, J. Catal. 234 (2005) 88–95.
[14] R. Xu, X. Wang, D.S. Wang, K.B. Zhou, Y.D. Li, J. Catal. 237 (2006) 426–430.
[15] G. Ertl, Proceedings of the Robert A. Welch Foundation Conferences on Chemical Research, Houston, Texas, November, 1981, pp. 9–11;
G. Ertl, Heterogeneous Catal. XXV (1981) 179.
[16] L. Zhang, D.R. Chen, X.L. Jiao, J. Phys. Chem. B 110 (2006) 2668–2673.
[17] Y. Zheng, F. Duan, J. Wu, L. Liu, M.Q. Chen, Y. Xie, J. Mol. Catal. A: Chem. 303 (2009) 9–14.
[18] J.Y. Kim, I. Chung, J.H. Choy, G.S. Park, Chem. Mater. 13 (2001) 2759–2761.
[19] Y. Tsunoda, W. Sugimoto, Y. Sugahara, Chem. Mater. 15 (2003) 632–635.
[20] L.G. Sillen, Naturwiss 30 (1942) 318–324.
[21] R.P. Turcotte, J.O. Sawyer, L. Eyrin, Inorg. Chem. 8 (1969) 238–246.
[22] D.O. Charkin, P.S. Berdonosov, A.M. Moisejev, R.R. Shagiakhmetov, V.A. Dolgikh, J. Solid State Chem. 147 (1999) 527–535.
[23] X. Zhang, Z.H. Ai, F.L. Jia, L.Z. Zhang, J. Phys. Chem. C 112 (2008) 747–753.
[24] J.D. Grice, Can. Mineral. 40 (2002) 693–698.
[25] R. Chen, M.H. So, J. Yang, F. Deng, H.Z. Sun, Chem. Commun. 21 (2006) 2265–2267.
[26] X.Y. Chen, H.S. Huh, S.W. Lee, J. Solid State Chem. 180 (2007) 2510–2516.
[27] E. Donath, B. Gleb, F. Carnso, Angew. Chem., Int. Ed. 37 (1998) 2201–2205.
[28] H. Shiho, N. Kawahashi, Colloid Polym. Sci. 278 (2000) 270–274.
[29] X.D. Song, F.Q. Zhao, Z.R. Liu, Y. Luo, Chem. J. Chin. Univ. 27 (2006) 125–128.
[30] A. Kudo, I. Tsuji, H. Kato, Chem. Commun. 17 (2002) 1958–1959.